ADVANCED MATERIALS INTERFACES
Open Access
www.advmatinterfaces.de

Check for updates

Slicing of 4H-SiC Wafers Combining Ultrafast Laser Irradiation and Bandgap-Selective Photo-Electrochemical Exfoliation

Wenhao Geng, Qinqin Shao, Yan Pei, Lingbo Xu, Can Cui, Xiaodong Pi, Deren Yang, and Rong Wang**

High-efficiency and low-loss processing is the mainstay to reduce the cost and deepen the application of 4H silicon carbide (4H-SiC) wafers in high-power and high-frequency electronics. In this study, the high-yield slicing of 4H-SiC wafers is realized by combining femtosecond laser irradiation and bandgap-selective photo-electrochemical (PEC) exfoliation. By combining light-absorption measurements, micro-Raman, and micro-photoluminescence characterizations, it is found that the damage layer formed inside 4H-SiC after femtosecond-laser irradiation consists of amorphous silicon and amorphous carbon. This indicates that the femtosecond-laser irradiation leads to phase separation in 4H-SiC. The bandgap of the damage layer is 0.4 eV. Taking advantage of the different bandgap energies of the damage layer and the perfect 4H-SiC region, the damage layer is removed from the perfect region of 4H-SiC by using bandgap-selective PEC etching. During the PEC etching, light-generated holes can selectively oxidize and corrode the damaged layer with the assistance of the HF solution, and leave the upper and lower perfect 4H-SiC layers being intact. The current work contributes to the development of the high-yield and high-throughput femtosecond laser slicing of 4H-SiC wafers.

1. Introduction

4H silicon carbide (4H-SiC) is one of the most promising wide-bandgap semiconductors for power electronics due to its high saturated electron velocity, high breakdown field, and strong chemical inertness.[1,2] 4H-SiC wafers are usually obtained from 4H-SiC single-crystal boules by using mechanical processes including wire sawing, grinding, lapping, and chemical-mechanical polishing (CMP). The sawing process significantly affects the yield and quality of 4H-SiC wafers.[3] The wire-sawing technique has been widely employed to slice 4H-SiC single-crystal boules to thin wafers and has realized mass production of semiconductor wafers due to its high throughput and high maturity.[3–5] However, the wire sawing of 4H-SiC wafers suffers from the problems of low efficiency and high material loss due to the high hardness and high brittleness of 4H-SiC.[6] The slurry wire sawing of a 6-inch. 4H-SiC boule often takes above 100 h.[7] Even though the diamond-wire sawing increases the sawing efficiency of 4H-SiC wafers, additional high-temperature annealing is usually required to repair the warpage of 4H-SiC wafers.[8] As to the material loss, the kerf loss of 4H-SiC material during the wire sawing is usually in the range of 150–180 μm per wire.[9] Furthermore, wire sawing creates high amount of surface damages and subsurface damages on 4H-SiC wafers, which should be removed by the followed grinding, lapping, and CMP.[10,11]

The ultrafast laser slicing has emerged as a technical

W. Geng, Q. Shao, X. Pi, D. Yang, R. Wang
State Key Laboratory of Silicon and Advanced Semiconductor Materials & School of Materials Science and Engineering
Zhejiang University
Hangzhou 310027, China
E-mail: xdpi@zju.edu.cn; rong_wang@zju.edu.cn

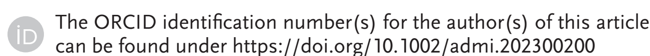

The ORCID identification number(s) for the author(s) of this article can be found under https://doi.org/10.1002/admi.202300200

© 2023 The Authors. Advanced Materials Interfaces published by Wiley-VCH GmbH. This is an open access article under the terms of the Creative Commons Attribution License, which permits use, distribution and reproduction in any medium, provided the original work is properly cited.

DOI: 10.1002/admi.202300200

W. Geng, Q. Shao, Y. Pei, L. Xu, X. Pi, D. Yang, R. Wang
Institute of Advanced Semiconductors & Zhejiang Provincial Key Laboratory of Power Semiconductor Materials and Devices
ZJU-Hangzhou Global Scientific and Technological Innovation Center
Zhejiang University
Hangzhou 311200, China
Y. Pei, L. Xu, C. Cui
Key Laboratory of Optical Field Manipulation of Zhejiang Province
Department of Physics
Zhejiang Sci-Tech University
Hangzhou 310018, China

 © 2023 The Authors. Advanced Materials Interfaces published by Wiley-VCH GmbH

21967350, 2023, 21, Downloaded from https://onlinelibrary.wiley.com/doi/10.1002/admi.202300200 by Xiamen University, Wiley Online Library on [11/04/2024]. See the Terms and Conditions (https://onlinelibrary.wiley.com/terms-and-conditions) on Wiley Online Library for rules of use; OA articles are governed by the applicable Creative Commons License

breakthrough for the high-efficiency and low-loss slicing of 4H-SiC wafers.[12,13] Under ultrafast laser irradiation, phase separation and defect generation occur in the focal depth of the untrafast laser. A thin damage layer is thus created inside the semiconductor single crystal by the ultrafast laser writing throughout the surface of the semiconductor.[14–16] The slicing of semiconductor wafers can be realized by exfoliating the damage layer from the perfect single-crystal region via mechanical stress, swelling stress, or thermal stress.[9,17,18] By replacing wire sawing with ultrafast laser slicing, the material loss and slicing duration per wafer are significantly reduced.[9,19] Moreover, the machining of ultrafast laser-sliced 4H-SiC includes only fine lapping and CMP, which further reduces the processing loss and improves the processing efficiency of 4H-SiC wafers.[19] By optimizing the parameters of the ultrafast laser, the thickness of the material loss can be reduced to ≈20 μm.[9,13] These advantages endow the ultrafast laser slicing a great potential in the high-efficiency and low-loss slicing of 4H-SiC wafers. However, the physical exfoliation often generates cracks or micro-cracks in the perfect region of 4H-SiC, which reduces the yield and hinders the application of ultrafast laser slicing of 4H-SiC wafers. Recently, photo-electrochemical (PEC) etching has attracted considerable attention as a bandgap-selective etching technique for separating III-V nitrides heterostructures with different compositions.[20–22] By selecting the wavelength of illumination that only generates electron–hole pairs in the narrower-bandgap III-V nitride, the photo-generated electrons transport to an external cathode and photo-generated holes participate in an oxidation reaction and initiate the etching of the narrower-bandgap III-V nitride. Since the ultrafast laser causes phase separation in the damage layer and changes the bandgap energy of the damage layer, the bandgap-selective PEC etching opens a pathway to exfoliate ultrafast laser-processed 4H-SiC wafers without introducing external stress, and fully explore the potential of ultrafast laser slicing of 4H-SiC wafers.

In this work, we realize the laser slicing of 4H-SiC wafers combining femtosecond laser irradiation and bandgap-selective PEC exfoliation. By combining light-absorption measurements, micro-Raman, and micro-photoluminescence (PL) characterizations, we find that the damage layer formed inside the 4H-SiC sample after femtosecond-laser writing consists of amorphous silicon and amorphous carbon. This indicates that the femtosecond laser irradiation causes phase separation and amorphization of 4H-SiC. The bandgap of the damage layer is 0.4 eV. Based on the different bandgap energies between the damage layer and the perfect 4H-SiC region, we propose to etch away the damage layer from the perfect region of 4H-SiC by bandgap-selective PEC etching. During the PEC etching, light-generated holes can selectively oxidize and corrode the damaged layer with the assistance of the HF liquid, and leave the upper and lower perfect 4H-SiC regions being intact. Our work opens a pathway to realize high-yield and high-throughput ultrafast laser slicing of 4H-SiC wafers, which holds great potential in the high-efficiency and low-loss processing of 4H-SiC wafers.

We first investigate the properties of the femtosecond-generated damage layer by mechanical exfoliation. The femtosecond laser irradiated 4H-SiC is separated into two samples under the mechanical exfoliation because the bonding of the interface between the damage layer and the perfect 4H-SiC region is weaker than that in the perfect 4H-SiC region. **Figure 1**a,b shows the 2D and 3D surface morphologies of one of the exfoliated samples. The overall surface roughness (R_a) of the exfoliated surface is 5 μm. The crystalline properties of the exposed damage layer are then investigated by micro-Raman spectroscopy. As shown in Figure 1c, the peak of the folded transverse optical (FTO) (776 cm^{-1}) mode of the exfoliated surface is slightly broadened and significantly weakened compared with that of the original 4H-SiC sample, which is probably due to the femtosecond-laser-writing induced residual strain.[23,24] Two broad Raman peaks centered at 480 and 1400 cm^{-1} are observed on the damage layer, which is attributed to the amorphous silicon and amorphous carbon, respectively.[9,25] Micro-PL observations indicate that the band-edge emission of 4H-SiC located at 390 nm is significantly weakened, as a result of residual strain-induced lattice distortion. Two broad PL peaks located at 425 and 500 nm are observed in the femtosecond-laser treated sample (Figure 1d), which respectively correspond to amorphous SiC_xO_y and amorphous carbon.[26,27] Therefore, both micro-Raman and mico-PL investigations indicate that the lattice distortion of 4H-SiC, as well as the phase separation from 4H-SiC to amorphous silicon and amorphous carbon, happens during the femtosecond laser irradiation, which agrees well with time-dependent density functional theory (TDDFT) simulations.[28]

Since the bandgap energies of amorphous silicon and amorphous carbon are both lower than that of 4H-SiC, we propose to separate the femtosecond laser writing induced damage layer from the perfect 4H-SiC region by bandgap-selective PEC. Before PEC experiments, the bandgap of the damage layer is evaluated by the Tauc plot method. The bandgap energy (E_g) is evaluated by

$$(\alpha h\upsilon)^{1/n} = A\left(h\upsilon - E_g\right) \quad (1)$$

where α is the absorption coefficient, h is the Planck constant, υ is the frequency, and A is a constant. Wherein, the exponent n of an indirect bandgap semiconductor is 2.[29,30] With the UV–vis spectra and Equation (1), the bandgap energy of the original 4H-SiC sheet is evaluated to be3.2 eV, which is consistent with theoretical and experimental results.[10,31] This verifies the validity of the Tauc plot method. With this approach, the bandgap energy of the femtosecond treated damage layer is estimated to be 0.4 eV as a result of the mixture of amorphous Si and amorphous C (**Figure 2**a). Before PEC etching, the femtosecond laser-induced damaged layer connects the perfect 4H-SiC region (Figure 2b). The wavelength of the light source during PEC etching is selected by the standard of $E_{g(\text{damage layer})} < h\nu < E_{g(\text{4H-SiC})}$, which promotes the bandgap-selective etching of the damage layer and intact preservation of the perfect 4H-SiC region. As shown in Figure 2c, the light source with a wavelength ranging from 400 to 800 nm is irradiated on the femtosecond laser-treated 4H-SiC sample, which generates the electron–hole pairs on the surface of the sample. A positive potential is applied to the 4H-SiC sample to separate the light-generated electron–hole pairs produced on the surface of the 4H-SiC sample. The light-generated electrons (e^-) are transferred to the cathode and participated in the hydrogen evolution by: $2H^+ + 2e^- \rightarrow H_2\uparrow$, while the remaining light-generated holes (h^+) participate in the oxidation and removal of the femtosecond

© 2023 The Authors. Advanced Materials Interfaces published by Wiley-VCH GmbH

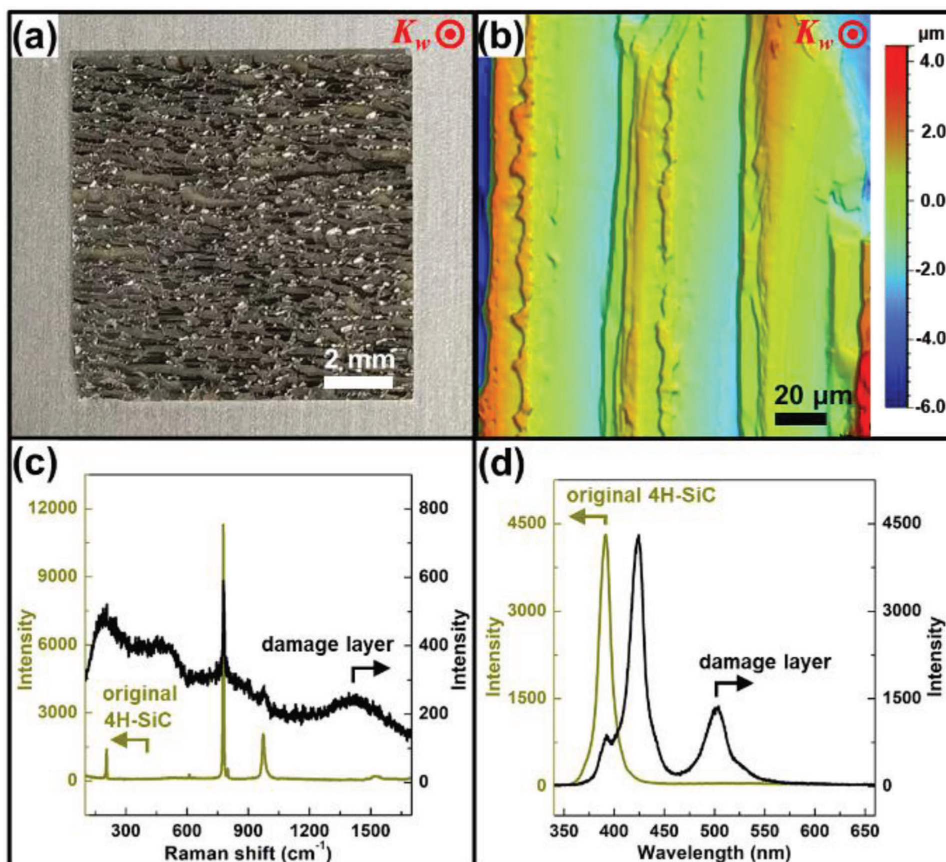

Figure 1. a) The photograph and b) the white light interferometry image of the mechanically exfoliated 4H-SiC sample. The red symbol of K_w shows the laser propagation direction. c) Micro-Raman spectra and d) Micro-PL spectra of the damage layer and the original 4H-SiC.

laser-induced damaged layer by the following reactions

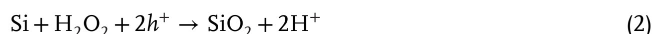

$$\mathrm{Si} + \mathrm{H_2O_2} + 2h^+ \rightarrow \mathrm{SiO_2} + 2\mathrm{H}^+ \quad (2)$$

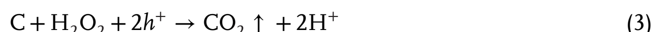

$$\mathrm{C} + \mathrm{H_2O_2} + 2h^+ \rightarrow \mathrm{CO_2} \uparrow + 2\mathrm{H}^+ \quad (3)$$

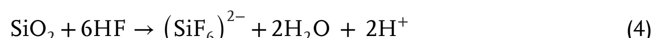

$$\mathrm{SiO_2} + 6\mathrm{HF} \rightarrow \left(\mathrm{SiF_6}\right)^{2-} + 2\mathrm{H_2O} + 2\mathrm{H}^+ \quad (4)$$

The potential applied is set as 2 V (vs counter electrode) to avoid the breakdown effects of 4H-SiC.[32,33] Because the oxidation and removal of the femtosecond laser-induced damaged layer only occur at the solid–liquid interface, the PEC etching firstly occurs around the damage layer and then gradually etch the damage layer inward the sample. In addition, the applied bias forms a drift current of the electrolyte within the narrow damage layer, this current delivers chemically active F^- radicals to the etch front, which accelerates the etching of the femtosecond laser-induced damaged layer.[34] The PEC etching of the femtosecond laser-irradiated 4H-SiC samples in the dark is also carried out for comparison. As shown in Figure 2d, the current density in the dark is relatively stable near 0.2 mA cm^{-2} for 180 min and the front surface has barely changed. This suggests that only the oxygen evolution occurs on the front surface of the 4H-SiC sample at 2 V. Once exposed to light irradiation, the PEC current density of 4H-SiC sheets increases instantaneously to 9 mA cm^{-2} at the initial stage and reaches a maximum of 16 mA cm^{-2} at 100 min. After 15 min of PEC etching, the edge of the amorphous layer obviously disappears and leaves a narrow etched slit (Figure 2e), whose thickness consists of the thickness (≈20 µm) of the femtosecond laser-induced damaged layer (Figure 2b). After 180 min of PEC etching under light irradiation, the PEC exfoliation is achieved and the 4H-SiC samples with smooth stripping surfaces with the R_a of 1 µm are obtained (Figure 2f).

The crystalline properties of the PEC-exfoliated surface are further investigated by micro-Raman and Micro-PL spectra. As shown in **Figure 3**a,b, the PEC-exfoliated sample shows the same Raman spectrum as the perfect 4H-SiC sample. In addition, the intensity mapping of the PL peak located at 390 nm covers the entire region (Figure 3c) and the variation of peak intensity is 11%. This indicates that the femtosecond laser-induced damage layer is totally removed and the perfect 4H-SiC region is preserved after PEC exfoliation.[35,36] In addition, the top surface of the 4H-SiC sample after 180 min PEC etching is extremely smooth, indicating that the top surface is preserved from PEC etching (Figure 3d). We note that the average etching rate of the PEC is about 0.33 cm^2 h^{-1}, which is limited by the mass transfer of the etching productions. When pushing the combination of femtosecond laser irradiation and bandgap-selective PEC exfoliation

© 2023 The Authors. Advanced Materials Interfaces published by Wiley-VCH GmbH

21967350, 2023, 21, Downloaded from https://onlinelibrary.wiley.com/doi/10.1002/admi.202300200 by Xiamen University, Wiley Online Library on [11/04/2024]. See the Terms and Conditions (https://onlinelibrary.wiley.com/terms-and-conditions) on Wiley Online Library for rules of use; OA articles are governed by the applicable Creative Commons License

21967350, 2023, 21, Downloaded from https://onlinelibrary.wiley.com/doi/10.1002/admi.202300200 by Xiamen University, Wiley Online Library on [11/04/2024]. See the Terms and Conditions (https://onlinelibrary.wiley.com/terms-and-conditions) on Wiley Online Library for rules of use; OA articles are governed by the applicable Creative Commons License

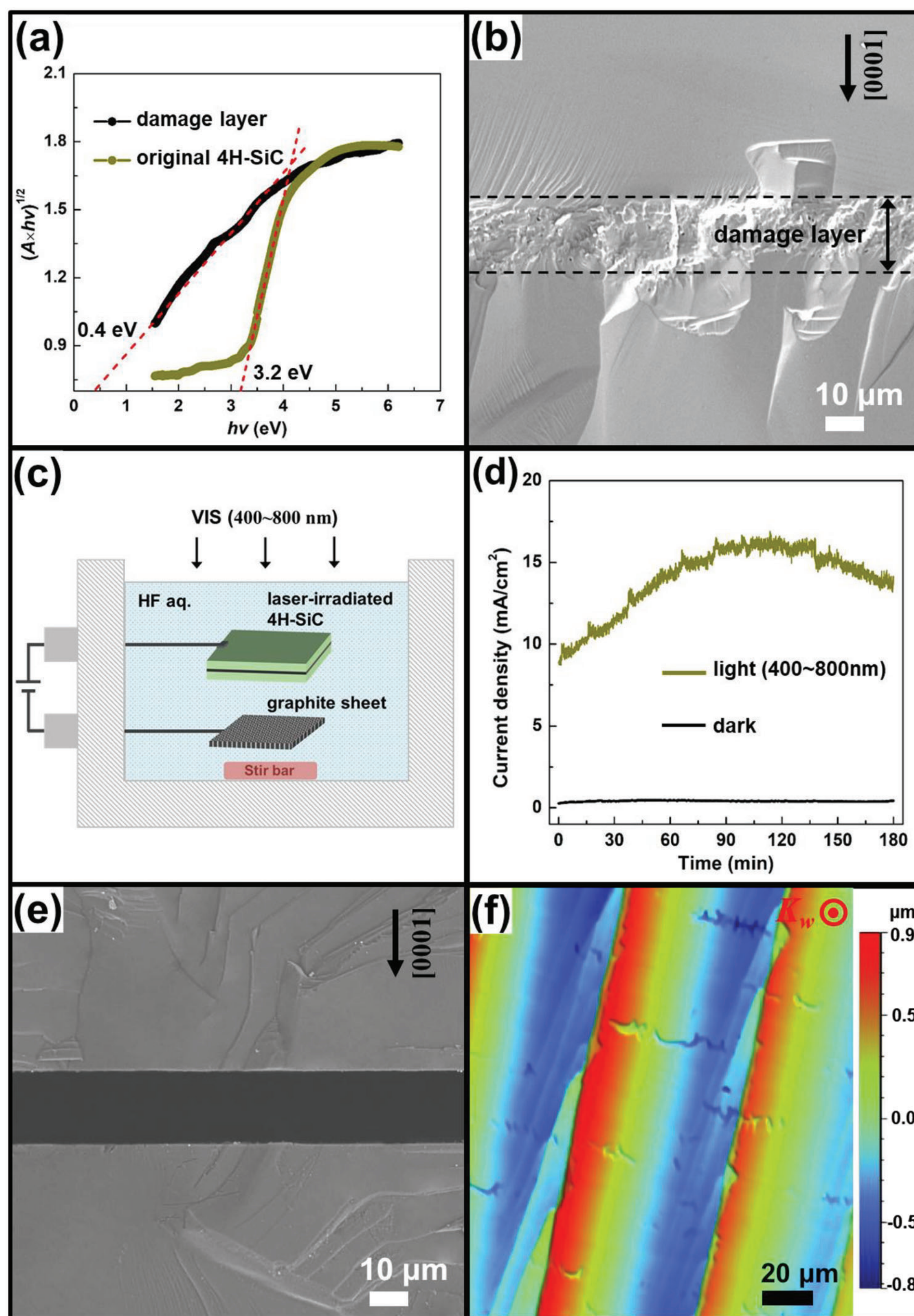

Figure 2. a) Tauc plots of perfect 4H-SiC and the femtosecond treated damage layer, b) cross-sectional SEM image of the femtosecond treated 4H-SiC sample, c) the schematic diagram showing the setup of the PEC etching of the femtosecond treated 4H-SiC sample, d) the current density during the PEC etching under light irradiation and dark environment, e) the cross-sectional SEM image of the 4H-SiC sample after 15 min of PEC etching, and f) the white light interferometry image of the exfoliated 4H-SiC sample after 180 min of PEC etching.

to the mass slicing of 4H-SiC wafers, microwave- or ultrasonic-assistant PEC etching and multi-wafer PEC etching systems are attractive to increase the production exfoliation of 4H-SiC wafers.

We have explored the nature of the pulsed femtosecond laser-treated 4H-SiC and revealed the validity of the PEC exfoliation of the pulsed femtosecond laser-treated 4H-SiC substrate. Light-absorption measurements, micro-Raman, and micro-PL characterizations indicate that the damage layer formed inside the 4H-SiC sample after femtosecond-laser writing consists of amorphous silicon and amorphous carbon. This indicates that the femtosecond-laser irradiation causes phase separation and amor-

© 2023 The Authors. Advanced Materials Interfaces published by Wiley-VCH GmbH

21967350, 2023, 21, Downloaded from https://onlinelibrary.wiley.com/doi/10.1002/admi.202300200 by Xiamen University, Wiley Online Library on [11/04/2024]. See the Terms and Conditions (https://onlinelibrary.wiley.com/terms-and-conditions) on Wiley Online Library for rules of use; OA articles are governed by the applicable Creative Commons License

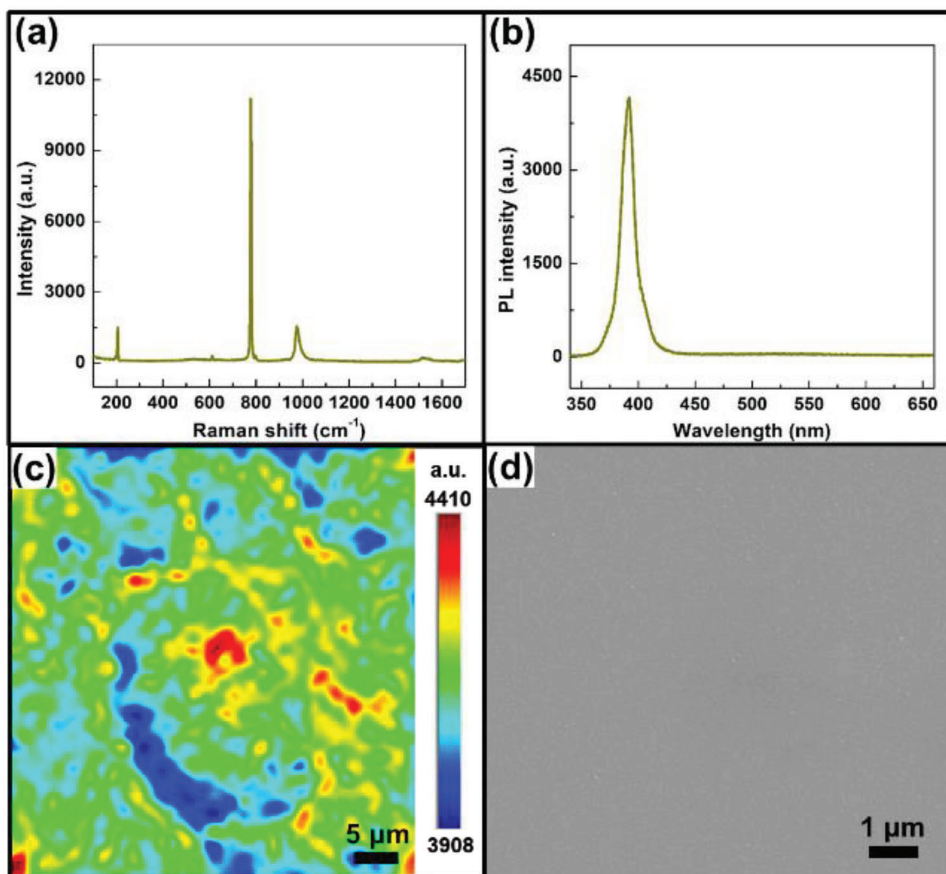

Figure 3. a) Micro-Raman spectrum and b) Micro-PL spectrum of the surface of the PEC exfoliated sample. c) Micro-PL mapping based on the intensity of peaks centered at 390 nm and d) the SEM images of the top surface of femtosecond laser-treated 4H-SiC after PEC etching.

phization of 4H-SiC. Taking advantage of the different bandgap energies between the damage layer and the perfect 4H-SiC region, we have etched away the damage layer from the perfect region of 4H-SiC by bandgap-selective PEC etching. During the PEC etching, light-generated holes can selectively oxidize and corrode the damaged layer with the assistance of HF liquid, and leave the upper and lower perfect 4H-SiC layers intact. Our work opens a pathway to realize high-yield and high-throughput ultrafast laser slicing of 4H-SiC wafers by combining ultrafast laser irradiation and bandgap-selective PEC exfoliation, which is attractive to the high-efficiency and low-loss processing of 4H-SiC wafers.

Experimental Methods: *n*-type 4H-SiC boules were grown by the physical vapor transport (PVT) technology.[37] 4H-SiC wafers with a thickness of 420 μm were processed by sequential wire sawing, lapping, and CMP,[11,38] and cut into 10 × 10 mm square samples. The center wavelength, pulse width, peak power, beam diameter, and repetition rate of the femtosecond laser used in this work were 1030 nm, 200 fs, 1×10^8 W, 1 μm, and 58 kHz, respectively. The femtosecond laser was focused at a depth of 210 μm inside the 4H-SiC sample along the [0001] direction. The laser-written tracks with a spacing of 20 μm were formed by scanning the wafer at the speed of 20 mm s^{-1}. The focus depth of the femtosecond laser was set as 210 μm in the 4H-SiC samples. The laser-irradiated 4H-SiC samples were sequentially washed with ultrasonic acetone, ethanol, and deionized water for 15 min, and finally immersed in the HF solution to remove surface oxides.

As shown in **Figure 4**, the exfoliation approaches of femtosecond laser-irradiated 4H-SiC samples include the traditional mechanical exfoliation and the PEC exfoliation that was proposed. For mechanical exfoliation, the sample was glued to the tooling with epoxy resin glue, and clamped by the SUS locking jig for curing. By using a universal testing machine, tensile stress was loaded in the normal direction relative to the sample surface to realize exfoliation.

The PEC etching was conducted in a two-electrode cell, in which the femtosecond laser irradiated 4H-SiC sample and the graphite sheet were used as working electrode and counter electrode, respectively. The voltage applied to the 4H-SiC sample was 2 V (vs counter electrode). A solution composed of C_2H_5OH (99% purity), HF (40% purity), H_2O_2 (30% purity), and deionized water with a volume ratio of 6:3:4:5 was employed as the electrolyte. The front sample surface was illuminated during the experiment. The 400 nm long pass filter (CEAULIGHT, UVIRCUT-400) was used to attenuate the UV light components of the radiation from a Xe light source (CEAULIGHT, CEL-HXUV300-T3), which formed the filtered spectrum ranging from 400 to 800 nm.

Characterizations: The surface morphologies of 4H-SiC samples after exfoliation were examined by a differential interference contrast (DIC) optical microscopy (OM) (Novel, NMM-820TRF),

© 2023 The Authors. Advanced Materials Interfaces published by Wiley-VCH GmbH

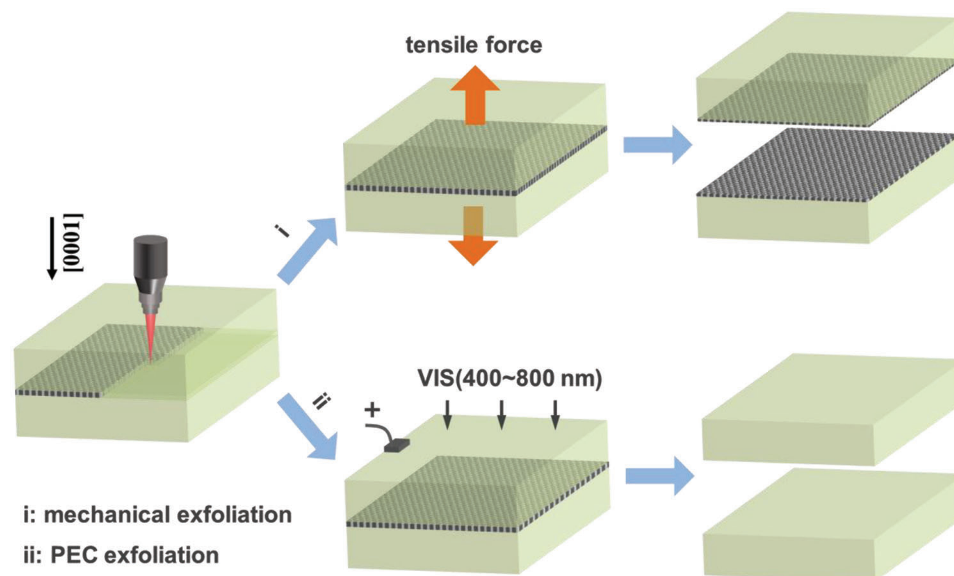

Figure 4. Schematic diagram showing the femtosecond laser writing and exfoliations: i) mechanical exfoliation, ii) PEC exfoliation.

a benchtop 3D optical profilometer (Bruker, ContourX-200), and scanning electron microscopy (SEM) (Zeiss, Sigma300). Micro-Raman spectroscopy and micro-photoluminescence spectroscopy were obtained by using the HORIBA LabRAM Odyssey, which was excited by lasers with wavelengths of 532 and 266 nm, respectively. The light absorption of 4H-SiC samples was recorded by a UV–vis spectrophotometer (Shimadzu, UV-3600Plus).

Acknowledgements

This work was supported by the National Natural Science Foundation of China (Grant No. 62274143), "Pioneer" and "Leading Goose" R&D Program of Zhejiang Province (Grant Nos. 2022C01021, 2023C01010), Fundamental Research Funds for the Central Universities (Grant No. 226-2022-00200), Natural Science Foundation of China for Innovative Research Groups (Grant No. 61721005), and Open Fund of Zhejiang Provincial Key Laboratory of Power Semiconductor Materials and Devices.

Conflict of Interest

The authors declare no conflict of interest.

Data Availability Statement

The data that support the findings of this study are available from the corresponding author upon reasonable request.

Keywords

4H silicon carbide wafers, ultrafast laser slicing, photo-electrochemical etching

Received: March 9, 2023
Revised: April 25, 2023
Published online: June 30, 2023

[1] P. J. Wellmann, *Semicond. Sci. Technol.* **2018**, *33*, 103001.
[2] X. Yang, R. Sun, K. Kawai, K. Arima, K. Yamamura, *ACS Appl. Mater. Interfaces* **2019**, *11*, 2535.
[3] H. Wu, *Precis. Eng.* **2016**, *43*, 1.
[4] J. Zhang, R. Zhu, X. Zhang, X. Zhang, Y. Gao, Y. Lu, X. Pi, D. Yang, R. Wang, *J. Synth. Cryst.* **2023**, *52*, 365.
[5] A. Bidiville, K. Wasmer, M. Van der Meer, C. Ballif, *Sol. Energy Mater. Sol. Cells* **2015**, *132*, 392.
[6] X. Liu, R. Wang, J. Zhang, Y. Lu, Y. Zhang, D. Yang, X. Pi, *J. Phys. D: Appl. Phys.* **2022**, *55*, 334002.
[7] A. R. Powell, *Wide Bandgap Semiconductors for Power Electronics: Materials, Devices, Applications*, (Eds: P. Wellmann, N. Ohtani, R. Rupp), Wiley, New York **2021**, pp. 33–46.
[8] X. Chen, X. Xu, X. Hu, J. Li, Y. Wang, S. Jiang, K. Zhang, M. Jiang, *Rare Met.* **2006**, *25*, 704.
[9] E. Kim, Y. Shimotsuma, M. Sakakura, K. Miura, *Opt. Mater. Express* **2017**, *7*, 2450.
[10] W. Geng, G. Yang, X. Zhang, X. Zhang, Y. Wang, L. Song, P. Chen, Y. Zhang, X. Pi, D. Yang, R. Wang, *J. Semicond.* **2022**, *43*, 102801.
[11] R. Zhu, F. Chen, X. Liu, W. Geng, X. Zhang, J. Yuan, R. Wang, D. Yang, X. Pi, Minimization of Lapping Loss toward low-cost 4H-SiC wafers, in preparation.
[12] E. Ohmura, K. Fukumitsu, M. Kumagai, H. Morita, *Trans. Jpn. Soc. Mech. Eng., Ser. C* **2008**, *74*, 446.
[13] E. Kima, Y. Shimotsuma, M. Sakakurab, K. Miura, *Proc. of SPIE* **2016**, *9983*, 40.
[14] M. Kumagai, N. Uchiyama, E. Ohmura, R. Sugiura, K. Atsumi, K. Fukumitsu, *IEEE Trans. Semiconduct. Manuf.* **2007**, *20*, 259.
[15] C. Gaudiuso, A. Volpe, A. Ancona, *Micromachines* **2020**, *11*, 327.
[16] Z. Zhang, Z. Wen, H. Shi, Q. Song, Z. Xu, M. Li, Y. Hou, Z. Zhang, *Micromachines* **2021**, *12*, 1331.
[17] A. Tanaka, R. Sugiura, D. Kawaguchi, T. Yui, Y. Wani, T. Aratani, H. Watanabe, H. Sena, Y. Honda, Y. Igasaki, H. Amano, *Sci. Rep.* **2021**, *11*, 17949.
[18] M. Swoboda, C. Beyer, R. Rieske, W. Drescher, J. Richter, *Mater. Sci. Forum* **2017**, *897*, 403.
[19] Disco corporation, ultra-fast laser slicing, https://www.discousa.com/kabra/index_eg.html#kabra_process, accessed: 1, **2023**.

© 2023 The Authors. Advanced Materials Interfaces published by Wiley-VCH GmbH

21967350, 2023, 21, Downloaded from https://onlinelibrary.wiley.com/doi/10.1002/admi.202300200 by Xiamen University, Wiley Online Library on [11/04/2024]. See the Terms and Conditions (https://onlinelibrary.wiley.com/terms-and-conditions) on Wiley Online Library for rules of use; OA articles are governed by the applicable Creative Commons License

[20] P. Ramesh, S. Krishnamoorthy, S. Rajan, G. N. Washington, *Appl. Phys. Lett.* **2014**, *104*, 243503.
[21] T. Yamada, Y. Ando, H. Watanabe, Y. Furusawa, A. Tanaka, M. Deki, S. Nitta, Y. Honda, J. Suda, H. Amano, *Appl. Phys. Express* **2021**, *14*, 036505.
[22] C. Youtsey, R. McCarthy, R. Reddy, K. Forghani, A. Xie, E. Beam, J. Wang, P. Fay, T. Ciarkowski, E. Carlson, L. Guido, *Phys. Status. Solidi B* **2017**, *254*, 1600774.
[23] S.-i. Nakashima, T. Mitani, M. Tomobe, T. Kato, H. Okumura, *AIP Adv.* **2016**, *6*, 015207.
[24] S. Nakashima, Y. Nakatake, H. Harima, M. Katsuno, N. Ohtani, *Appl. Phys. Lett.* **2000**, *77*, 3612.
[25] J. Schwan, S. Ulrich, V. Batori, H. Ehrhardt, S. R. P. Silva, *J. Appl. Phys.* **1996**, *80*, 440.
[26] S. Gallis, V. Nikas, H. Suhag, M. Huang, A. E. Kaloyeros, *Appl. Phys. Lett.* **2010**, *97*, 081905.
[27] M. Li, L. Jiang, Y. Peng, T. Wang, T. Xiao, P. Xiang, X. Tan, *Optik* **2019**, *176*, 401.
[28] I. Choi, H. Y. Jeong, H. Shin, G. Kang, M. Byun, H. Kim, A. M. Chitu, J. S. Im, R. S. Ruoff, S. Y. Choi, K. J. Lee, *Nat. Commun.* **2016**, *7*, 13562.
[29] L. Zhang, J. Ran, S. Z. Qiao, M. Jaroniec, *Chem. Soc. Rev.* **2019**, *48*, 5184.
[30] S. Xu, F. Jiang, F. Gao, L. Wang, J. Teng, D. Fu, H. Zhang, W. Yang, S. Chen, *ACS Appl. Mater. Interfaces* **2020**, *12*, 20469.
[31] D. Stefanakis, K. Zekentes, *Microelectron. Eng.* **2014**, *116*, 65.
[32] Y. Chen, C. Zhang, L. Li, S. Zhou, X. Chen, J. Gao, N. Zhao, C. P. Wong, *Small* **2019**, *15*, 1803898.
[33] Y. Shishkin, W. J. Choyke, R. P. Devaty, *J. Appl. Phys.* **2004**, *96*, 2311.
[34] R. P. Strittmatter, R. A. Beach, T. C. McGill, *Appl. Phys. Lett.* **2001**, *78*, 3226.
[35] M. Bauer, A. M. Gigler, A. J. Huber, R. Hillenbrand, R. W. Stark, *J. Raman Spectrosc.* **2009**, *40*, 1867.
[36] H. Harima, S. i. Nakashima, T. Uemura, *J. Appl. Phys.* **1995**, *78*, 1996.
[37] N. Zhang, Y. Gao, R. Zhu, R. Wang, D. Yang, X. Pi, *J. Cryst. Growth* **2022**, *600*, 126915.
[38] X. Zhang, X. Liu, Y. Wang, R. Zhu, X. Zhang, Y. Zhang, R. Wang, D. Yang, X. Pi, *Semicond. Sci. Technol.* **2023**, *38*, 034001.

© 2023 The Authors. Advanced Materials Interfaces published by Wiley-VCH GmbH

21967350, 2023, 21, Downloaded from https://onlinelibrary.wiley.com/doi/10.1002/admi.202300200 by Xiamen University, Wiley Online Library on [11/04/2024]. See the Terms and Conditions (https://onlinelibrary.wiley.com/terms-and-conditions) on Wiley Online Library for rules of use; OA articles are governed by the applicable Creative Commons License